Review of Scientific Instruments

RESEARCH ARTICLE | FEBRUARY 07 2025

A high bandwidth and high transmission STM bias line for ESR and quantum stochastic resonance measurements at 0.4 K

Johannes Schwenk ; Clément M. Soulard ; Shixuan Shan ; François Patthey ; Harald Brune

Rev. Sci. Instrum. 96, 023706 (2025)
https://doi.org/10.1063/5.0228393

Review of Scientific Instruments ARTICLE pubs.aip.org/aip/rsi

A high bandwidth and high transmission STM bias line for ESR and quantum stochastic resonance measurements at 0.4 K

Cite as: Rev. Sci. Instrum. 96, 023706 (2025); doi: 10.1063/5.0228393
Submitted: 12 July 2024 • Accepted: 22 December 2024 •
Published Online: 7 February 2025

Johannes Schwenk,[a),b)] Clément M. Soulard, Shixuan Shan, François Patthey, and Harald Brune[a)]

AFFILIATIONS

Institute of Physics, EPFL, CH-1015 Lausanne, Switzerland

[a)]**Authors to whom correspondence should be addressed:** johannes.schwenk@kit.edu and harald.brune@epfl.ch
[b)]**Present address:** Physikalisches Institut, Karlsruhe Institute of Technology, D-76131 Karlsruhe, Germany.

ABSTRACT

We present a scanning tunneling microscope operating in a ^{3}He cryostat at a base temperature of 0.4 K, suitable for electron spin resonance (ESR) [S. Baumann, W. Paul, T. Choi, C. P. Lutz, A. Ardavan, and A. J. Heinrich, Science **350**, 417 (2015)], quantum stochastic resonance (QSR) [M. Hänze, G. McMurtrie, S. Baumann, L. Malavolti, S. N. Coppersmith, and S. Loth, Sci. Adv. **7**, eabg2616 (2021)], and electric pump–probe experiments. We achieve excellent signal transmission of −2 to −3 dB between 100 kHz and 100 MHz, −23 dB at 10 GHz, −35 to −40 dB between 25 and 35 GHz, and −45 dB at 40 GHz, using a combination of normal conducting and superconducting semi-rigid, as well as flexible RF cables. SMK type 2.92 mm and mini-SMP connectors are used to minimize reflections and losses over the entire frequency range. The ESR capability of our instrument is demonstrated on possibly hydrogenated titanium atoms adsorbed on two and three monolayers of MgO on Ag(100) at 0.4 and at 4.2 K. We further show QSR measurements for Fe/MgO/Ag(100) and compare the driven relaxation time with the intrinsic energy relaxation time T_1 reported for that system [W. Paul, K. Yang, S. Baumann, N. Romming, T. Choi, C. P. Lutz, and A. J. Heinrich, Nat. Phys. **13**, 403 (2017)] as a function of magnetic field and tunnel current.

I. INTRODUCTION

The combination of electron spin resonance (ESR) and scanning tunneling microscopy[1–7] provides the necessary tool to locally manipulate and measure quantum spin states. It requires a modulation of the tip–sample bias, typically in the frequency range of a few GHz up to tens of GHz, depending on the g-factor of the spin system, the operating temperature of the microscope, and the externally applied magnetic field. In some previously realized setups, this RF modulation is realized by antennae, where the microwave radiation is propagating through the vacuum to the tip–sample junction,[5–7] while others implement an RF compatible bias line contacting the tip or the sample of the scanning tunneling microscope (STM).[1,3,4,7,8] Purely antenna based setups typically exhibit a gap in the frequency range of possible bias modulations since their transmission range often starts at frequencies significantly above the bandwidth of the regular bias line. On the other hand, setups with wire-based RF contacts sometimes exhibit poor RF transmission, that is, for some frequencies, not sufficient for usable bias modulations at the tunnel junction.[3,4] In this article, we present a new cryogenic and RF compatible wiring of our existing STM system,[3,9,10] providing direct contact to the STM tip and allowing for modulations at arbitrary frequencies up to 40 GHz.

Although designed with ESR–STM measurements in mind, our experimental setup presented in Sec. II is also ideally suited for stochastic resonance measurements. Stochastic resonance can provide a measure of the characteristic time scale of bi-stable systems. In Ref. 11, the authors demonstrate quantum stochastic resonance (QSR) and measure the characteristic switching time of the spin of a single Fe atom adsorbed on a $Cu_2N/Cu(100)$ surface. Recently, the switching response of binary orbital memory states in Fe and Co atoms on black phosphorus to a sinusoidal drive has been studied in Ref. 12, where the authors investigate the influence of the

measurement parameters on the frequency dependent time average occupation of the system. Here, we employ this technique to investigate the spin dynamics of single Fe atoms on the MgO/Ag(100) surface and compare our results with the energy relaxation time T_1 measured in a previous study by electric pump–probe spectroscopy.[13]

II. SETUP

A. STM system

Our existing STM[3,9,10] is mounted in a custom single shot ^{3}He cryostat, operating at a base temperature below 0.4 K and under UHV conditions. The system is equipped with a superconducting vector magnet with a field of up to 8 T perpendicular and up to 0.8 T parallel to the sample surface. The insert of the cryostat has a separate ^{4}He bath, thermally decoupled from the main ^{4}He bath hosting the magnet. This allows for variable temperature measurements from 0.4 up to 50 K.[14] However, it also implies filling the insert's ^{4}He bath every 20 h. Inserting the ^{4}He transfer line into the insert causes mechanical vibrations, requiring the tip to be retracted by the coarse motion system and making it difficult to remain on the same surface spot and/or to keep the same tip apex between successive fillings of the insert. An improved thermal anchoring of the radiation shields, as well as a complete rewiring of the insert with superconducting NbTi cables between the 4.2 K stage and the ^{3}He pot, extended the ^{3}He single-shot hold time from ~12 to 21 h. During the reinitialization of the ^{3}He single shot mode, while re-condensing the ^{3}He, the STM temperature remains below 4.2 K. The outer radiation shield of the cryostat is cooled by liquid nitrogen, which is pumped and solidified to make STM measurements feasible, limiting uninterrupted stable measurement conditions to about 14 h.

B. Electronics

Figure 1 shows a schematic of the electronic setup used for the control of the STM and for applying the combined DC and RF bias to the STM tip (RF bias line). We use our own Python libraries[15,16] on the control PC to configure the RF[17] and the arbitrary waveform generator (AWG),[18] as well as the Nanonis SPM control software.[19] All measurements shown below are recorded using the RF generator.[17] During the measurements, a hardware trigger synchronizes the output of the generators with the data acquisition at each data point. The RF signal is modulated in a square on–off pattern at a frequency of 323 Hz using the generator's internal modulation. The resulting modulation of the tunneling current ΔI represents the difference in tunneling current with and without applied RF modulation and is detected using the digital lock-in module of the SPM control system.[20]

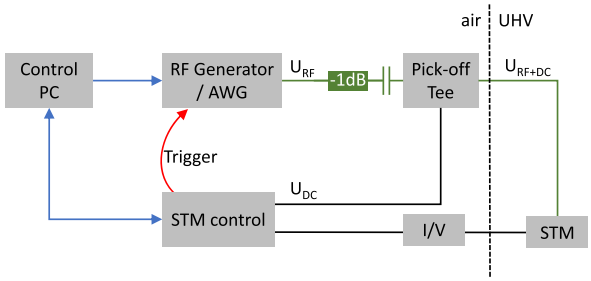

FIG. 1. Electronic control setup used for ESR and QSR measurements. Network connections (blue) link the control PC to the STM control system,[20] an analog RF-generator,[17] and an AWG.[18] 40 GHz RF components and cables are drawn in green, and coaxial cable connections for signals with AC components up to 10 kHz are in black.

C. RF bias line

Standard 50 Ω flexible RF cables with SMK type 2.92 mm connectors[21] establish the connection between the RF-generator or the AWG and the vacuum system over a total length of 6 m. A DC block[22] protects the output of the RF-generator, and a 1 dB attenuator[23] mitigates voltage pulses that occur when the generator's internal attenuation is switched. As illustrated in Fig. 1, the tunneling bias is added to the signal via a pickoff tee.[24]

The wiring for all STM signals, including the new RF bias line, inside the UHV chamber is guided along the translatable cryostat insert described in Refs. 3 and 9, requiring a total length of ~1.6 m. The RF bias line to the STM tip, illustrated in Fig. 2, is comprised

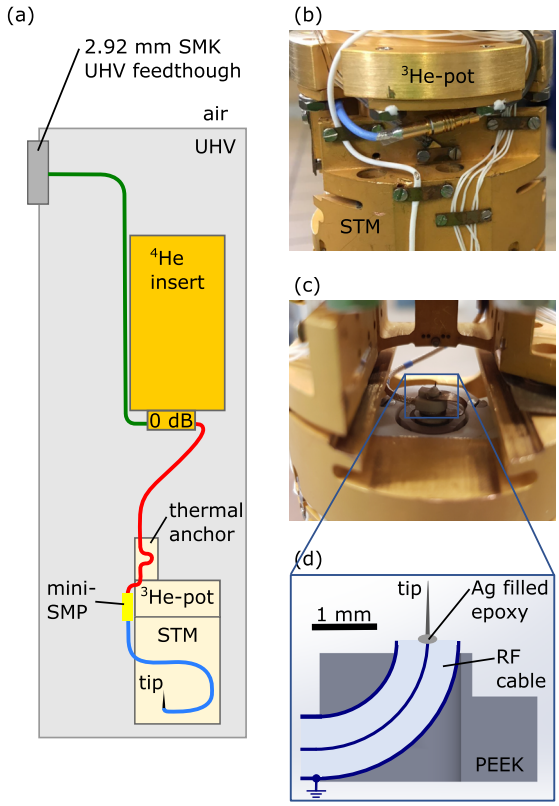

FIG. 2. (a) Illustration of the RF bias line along the cryostat insert and in the STM. Green: semi-rigid stainless steel cable with silver coated center conductor,[26] red: semi-rigid superconducting NbTi cable,[27] and blue: flexible RF cable.[29] (b) The mini-SMP connector visible in the center of the photograph connects the blue flexible RF cable to the NbTi semi-rigid line. (c) View of the STM tip with no sample installed. The PEEK guiding part is visible in the center, clamped onto the piezo tube. (d) Sketch of the PEEK guiding part, which is clamped on top of the piezo tube, supporting the RF cable with the STM tip glued to its end.

of three parts described below. All connectors and components are chosen to be compatible up to a frequency of 40 GHz. We use a CF-40 UHV feed-through with 2.92 mm SMK type bulk head connectors.[25] On the UHV side of the feed-through, a semi-rigid cable[26] of ~1.2 m in length is connected and guided through the cryostat to the 4.2 K stage. Here, it is connected to a thermally anchored 0 dB attenuator, ensuring a good thermal coupling of the cable's shield and center conductor to the insert's ^{4}He bath. SMK type 2.92 mm connectors are soldered to the cable on both ends using Pb- and flux-free Sn_{96} Ag_4 solder together with Castolin 157 inorganic flux, which is thoroughly rinsed off in an ultrasonic bath after each soldering step. Following the 4.2 K stage, a superconducting semi-rigid NbTi cable[27] with a length of ~0.3 m brings the RF bias line to the ^{3}He stage, ensuring minimum heat conduction and dissipation of RF power. Silver-filled epoxy resin[28] is used to thermally anchor the NbTi cable to the ^{3}He pot and to attach an SMK type 2.92 mm connector on the top end as well as a mini-SMP connector located at the STM body [see Fig. 2(b)]. The contact of the RF bias line to the STM tip is made by a 0.1 m flexible RF cable[29] with a silver coated copper core and a double shield with a silver plated helical foil and silver plated wire braid, which is soldered to the mini-SMP connector as shown in the photograph in Fig. 2(b). In the last section of the cable, the outer insulation layer is removed in order to increase its flexibility. The end of the cable is held by a guiding piece, made of polyether ether ketone (PEEK), which is clamped to the top of the piezo tube, used for scanning and z-motion of the tip, such that the entire cable can be removed *ex situ* to install an STM tip [see Figs. 2(c) and 2(d)]. The cable is fixed with a sharp 90° bend such that its end is pointing perpendicular to the sample, and the tip is glued to the center conductor with electrically conductive silver-filled epoxy resin.[28] This assembly preserves the impedance matching geometry of the RF cable and, thus, minimizes reflections of the RF power before the open end at the STM tip. The tip is made by electro-chemical etching of a Pt_{90} Ir_{10} wire of 0.25 mm diameter and about 2 mm length.

The mechanical stability of the STM was not affected negatively by the installation of the RF cable. For instance, in traces of the apparent height z recorded with a spin-polarized tip above magnetic atoms in order to monitor their magnetization switching, we observed a peak-to-peak noise of 0.7 ± 0.1 pm after having installed the RF cable compared to 1.7 ± 0.4 pm measured prior to the upgrade (both numbers refer to a 3 Hz Butterworth filter). The maximum power spectral density (PSD) after the upgrade was found to be 4.3 pA/Hz$^{1/2}$ (1.1 pm/Hz$^{1/2}$) at 545.9 Hz with a gated feedback loop (tunneling conditions before turning off feedback: V_{DC} = 100 mV and I_t = 100 pA). The average PSD of the system is lower than 400 fA/Hz$^{1/2}$ (100 fm/Hz$^{1/2}$).

III. RESULTS

A. RF transmission

The transmission of the RF power from the RF generator to the STM tunnel junction depends on the frequency and needs to be compensated in order to achieve a constant amplitude RF bias modulation V_{RF} at the STM junction for different frequencies f. We define the transfer-function TF as the transmission of our RF bias line in dB, given by

$$TF(f) = V_{dB}^{jun} - V_{dB}^{src} = 20 \cdot \log_{10}\left(V_{RF}/V^{src}\right), \quad (1)$$

where V_{RF} is the zero to peak amplitude of the RF modulation at the STM tunnel junction, V^{src} is the zero to peak amplitude at the RF generator, and V_{dB}^{jun} and V_{dB}^{src} are the respective amplitudes expressed in dB. We characterize $TF(f)$ by measuring the rectified current induced by an RF modulation voltage V_{dB}^{jun} of 20 dBmV when applied over a non-linear I–V-characteristic[1] at a temperature of 4 K. In the frequency range of 10 kHz to 10 GHz, we use the spin excitation step at ±14 meV of an Fe atom adsorbed on MgO/Ag(100)[30] and get the transmission shown in Fig. 3(a). The transmission in the range

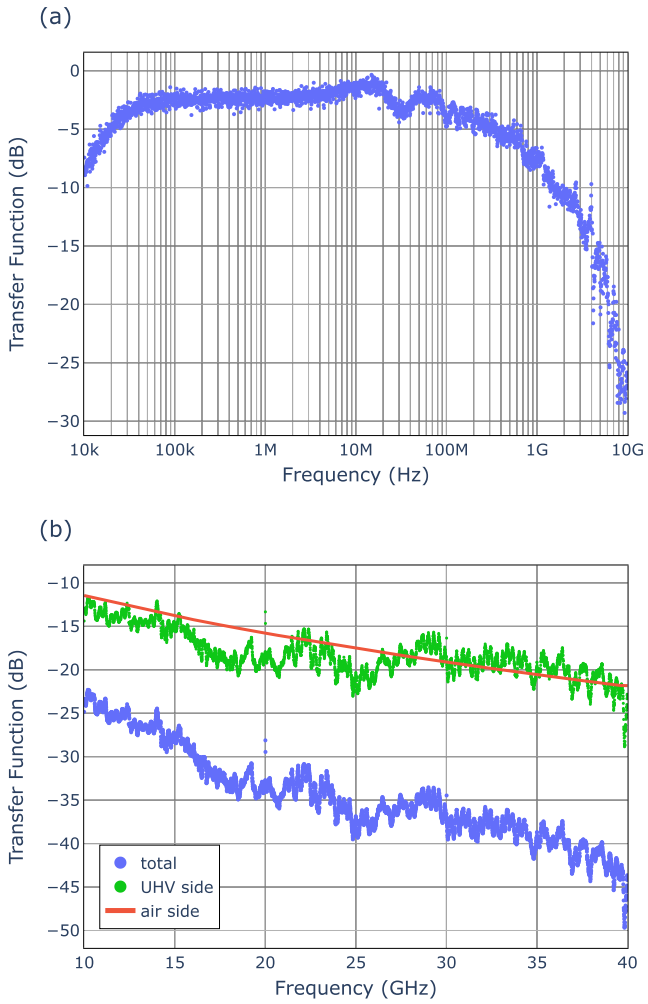

FIG. 3. RF transfer function of the STM setup: (a) measured in the range of 10 kHz–10 GHz utilizing the non-linearity of the spin excitation step of an Fe atom on MgO/Ag(100) and (b) measured from 10 to 40 GHz using the surface state onset of Ag(111). The blue symbols show the data measured for the complete setup, and the red line is an estimation of the transmission of all components in air, between the RF generator and the UHV feedthrough. The green symbols show the estimated transmission from the 300 K flange to the tunneling junction, obtained by subtracting the air-side losses (red) from the total transfer function (blue). Both transfer functions are obtained at T = 4 K and B_z = 0.5 T for V_{dBmV}^{jun} = 20 dBmV.

of 10–40 GHz is determined using the onset of the Ag(111) surface state[31,32] and plotted in Fig. 3(b). The initially lower transmission at frequencies below ~40 kHz stems from the DC block in the signal path (see Fig. 1), leading to an AC coupling between the RF generator and the STM tunnel junction. Starting from a frequency of about 100 MHz, losses in the cables become more significant. The red line in Fig. 3(b) indicates the losses that are expected from the air side components, 6 m of *Duratest* 150 cable[21] and the 1 dB attenuator.[23] Note that the air side wiring in our setup contributes significantly to the overall RF losses. However, those losses do not affect the measurement performance, since the suitable RF cables do not exhibit sudden changes in the transmission as a function of frequency. Air side losses, contrary to the ones occurring at low temperature stages, do not lead to any heating of the STM. In order to facilitate a comparison of different setups, we estimate the transfer function of our UHV RF wiring by subtracting the loss of the air side components [Fig. 3(b), green symbols]. The transmission of the entire RF bias line follows the general trend of the frequency dependent transmission expected from standard RF cables with losses between roughly 12 and 24 dB caused by the UHV wiring. The change of the ^{4}He filling level of the cryostat insert over time on the order of 1 cm/h leads to a change of the temperature profile of the stainless steel RF cable[26] between room temperature and the 4 K stage [cf. Fig. 2(a)]. Since the attenuation of the cable at 4 K decreases by more than a factor of 2 compared to room temperature, we observe variations of the transfer function of up to 3 dB, depending on the insert's ^{4}He filling level. This is the reason for the slightly different values of the transfer function at 10 GHz in panels (a) and (b) of Fig. 3. The overall shape and characteristic features of the transfer function are not influenced by this effect. The transmission of our RF line is better than the TF published for systems where the tip or sample is contacted[4,33,34] and comparable with the best TF reported for an antenna setup.[5]

B. ESR measurements

In order to benchmark the ESR measurement capability of our STM, we deposit single Fe and Ti atoms with a coverage of less than 1% of a monolayer at $T < 10$ K on an MgO film grown on Ag(100). Under these conditions, the atoms adsorb as single atoms on the MgO thin film. Spin polarization and ESR activity of the STM tip are achieved by picking up single Fe atoms from the MgO[2] after gently indenting the tip into the Ag surface to prepare a tip apex with the desired spatial resolution. ESR frequency sweeps are recorded on a bridge site Ti atom at a temperature of 0.4 K [Fig. 4(a)] as well as on an oxygen top site Ti atom at 4.2 K [Fig. 4(b)]. Changes in the temperature profile of the stainless steel semi-rigid RF wire lead to a time dependent transmission, such that the amplitude variations of the RF modulation are not fully compensated. The resulting background signal variation in the frequency sweeps, plotted in orange, is obtained from the average of all four sweeps at different in-plane B-fields, excluding the respective resonance peaks. This background is subtracted from the four frequency sweep data traces. The black lines show fits of the data with a Fano line shape.[35,36] The Fano factor q depends on the amplitude of the RF modulation and the DC tunneling current. Since these parameters are identical for all measurements in Figs. 4(a) and 4(b), respectively, we allow only one value of q optimized for all four frequency sweep traces by minimizing the sum of residuals for the entire dataset. A linear fit of the peak

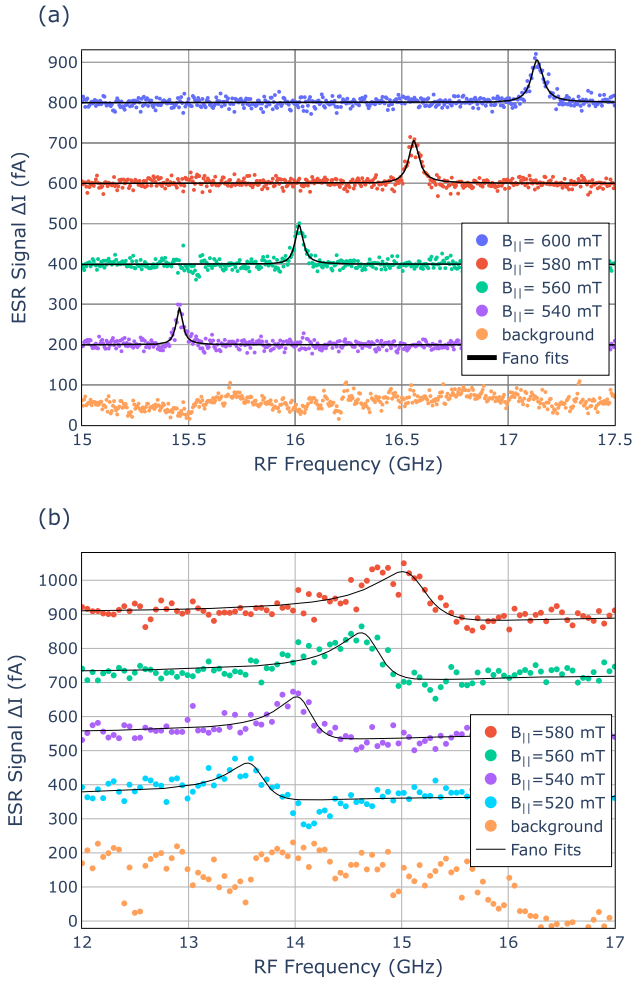

FIG. 4. Frequency sweeps on Ti on MgO/Ag(100). Plots are offset for clarity except for the background signals (orange symbols). (a) Measured on bridge site Ti at $T = 0.4$ K with a bias of $V_{DC} = 60$ mV, an RF junction amplitude of $V_{RF} = 28$ mV, and $I_t = 15$ pA current setpoint. Fano factor used in fits: $q = -0.027$. (b) Measured on a Ti adsorbed on the oxygen top site at $T = 4.25$ K with a bias of $V_{DC} = 100$ mV, an RF junction amplitude of $V_{RF} = 28$ mV, and $I_t = 27$ pA current setpoint. Fano factor: $q = 0.384$.

positions at 0.4 K yields a g-factor of $g = 1.99 \pm 0.02$ and a tip magnetic stray field of $B_{tip} = 15 \pm 4$ mT, in good agreement with previous results.[3,5,37–41] The peak amplitude is around 100 fA, corresponding to 0.7% of the current setpoint, and the smallest peak width is 37 ± 3 MHz. The first value characterizes how much ESR signal a given tip produces, which sensitively depends on the shape and composition of the tip–apex, yielding the gradient of the stray field and the spin-contrast. Our value is smaller than the best reported ones, e.g., 3%.[42] The second value contains decoherence effects but also measurement artifacts. For instance, atom tracking can lead to larger peak widths since varying the lateral position of the STM tip varies the stray field at the atom and thereby influences the ESR resonance frequency.[43] At 4.25 K, the ESR peaks are still nicely resolved. The data were recorded above a Ti atom on an oxygen site for which we find

$g = 1.82 \pm 0.09$ and $B_{tip} = 15 \pm 29$ mT. The large uncertainty of B_{tip} is due to deviations of the data from the linear fit and due to the larger error bar of the individual resonance frequencies due to the broader peaks. We note that different atoms show slightly different g- and B_{tip}-values, presumably due to defects in their vicinity.

C. QSR measurements

The electronic setup and signal detection for our QSR is identical to the one used for ESR measurements, described in Sec. II B and shown in Fig. 1. The RF generator[17] can provide a minimum modulation frequency of 9 kHz and is used for the measurements shown here. For lower modulation frequencies, our arbitrary waveform generator[18] can be used in a range from DC to ~1 GHz. The demodulated current signal ΔI is recorded in a logarithmic frequency sweep of the modulation frequency with a constant amplitude V_{RF} at the STM tunnel junction. The sweeps are typically carried out from 10 kHz to 1 GHz, while the tip is positioned over the Fe atom. ΔI is plotted in Fig. 5 for a spin averaging tip (red) that remains flat over the entire frequency range. The same signal recorded with a spin polarized tip (Fig. 5, blue symbols) is well fitted by a Lorentzian line shape (black dots in Fig. 5), centered at 0 Hz with a width of $f^* = 170 \pm 2$ kHz.

In the case of a spin polarized tip, ΔI is a measure of the relative change in average population of the Fe atom's magnetic ground state $|0\rangle$ and its first excited state $|1\rangle$ induced by the on–off chopping scheme of the bias modulation (the labeling refers to the one of Refs. 2 and 30, i.e., in a magnetic field pointing up, $|0\rangle$ corresponds to $\langle S_z\rangle = 2$ and $|1\rangle$ to $\langle S_z\rangle = -2$). For the present tip, the tunnel magnetoresistance is higher for state $|0\rangle$ than for state $|1\rangle$; therefore, the current decreases once the excited state $|1\rangle$ gets more populated. At sufficiently high modulation frequency, the Fe atom remains in state $|1\rangle$ during the bias modulation cycle. The frequency f^* corresponds to the most abundant switching frequency between $|0\rangle$ and $|1\rangle$.[11] Van Weerdenburg *et al.*[12] show that the change in time average occupation in an AC driven two state system occurring at f^* is caused by the voltage dependence of the switching rates and is a measure of the system's average switching time.

The energy relaxation time T_1 of Fe was reported in pump–probe measurements to scale linearly with the external out-of-plane magnetic field up to 2 T.[13] For higher B-fields, T_1 saturates at around 3 ms. Pump–probe measurements are different from QSR, as the latter applies a continuous drive, implying more electron scattering. Therefore, it is interesting to compare $\tau^*/2$ obtained under these conditions with T_1. Figure 6(a) shows the normalized ΔI signal as a function of an out-of-plane external magnetic field. Note that the spin-contrast is inverted with respect to Fig. 5; the ground state has less conductance than the excited state, i.e., the tunnel current increases once we hit the resonance. We use the widths f^* of Lorentzian fits of the data, centered at zero frequency, as a measure of the average time scale of the Fe spin switching, given by $\tau^*/2 = 1/(2f^*)$. It is plotted in Fig. 6(b) and shows a plateau at ~1.5 μs for $B_z > 2$ T, in qualitative agreement with the results for T_1 reported by Paul *et al.*[13] The quantitative difference between $\tau^*/2$ and T_1 can be explained by the ~100 times higher tip–sample conductance and, consequently, higher scattering by tunnel electrons. The generally lower times found here for $\tau^*/2$ are expected since during the delay time of the pump–probe measurements,[13]

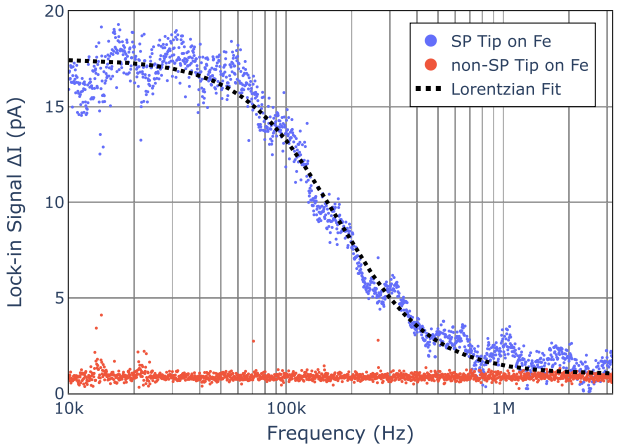

FIG. 5. QSR measurements with a spin-averaging tip (red) and a spin-polarized tip positioned over an Fe atom on two ML of MgO in a perpendicular magnetic field $B_z = 2.5$ T. The bias applied to the tunnel junction is $V_{DC} = -10$ mV with a modulation of $V_{RF} = 10$ mV; $T = 0.4$ K and $I_t = 400$ pA.

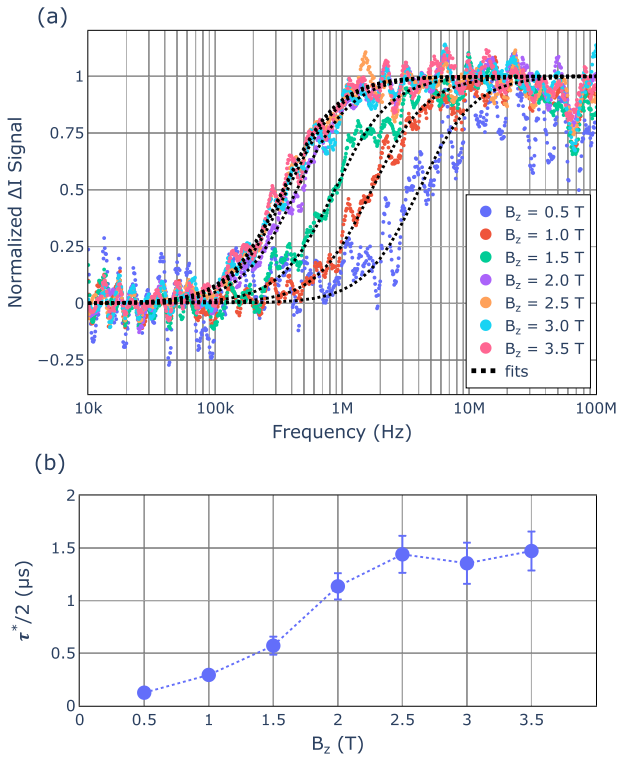

FIG. 6. (a) QSR measured with a spin polarized tip on an Fe atom on three ML of MgO at different external magnetic fields B_z applied perpendicular to the sample surface. The plots are smoothed for clarity; the dashed lines show Lorentzian fits of the raw data ($T = 0.4$ K, $V_{DC} = -10$ mV, $V_{RF} = 10$ mV, and $I_{set} = 200$ pA). (b) Magnetic field dependence of the characteristic time scale of the Fe spin switching $\tau^*/2$, derived from the half width at half maximum of the Lorentzian fits in panel (a).

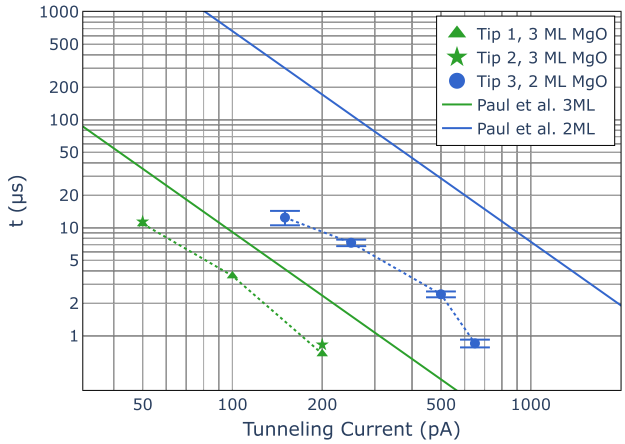

FIG. 7. The symbols show $\tau^*/2$ obtained from QSR measurements at different tunneling currents, with $B_z = 1.5$ T, $T = 0.4$ K, $V_{DC} = -10$ mV, and $V_{RF} = 10$ mV. Data shown in green are measured on three ML of MgO, and the data in blue on two ML. For tips 1 and 2, the errors are smaller than the symbols in the plot. The lines indicate an extrapolation of T_1, measured by Paul *et al.* in Ref. 13 at $B_z = 5$ T and $T = 1.2$ K.

the tip–sample bias is zero, while for the QSR measurements, the DC and AC bias modulation is continuously applied. Thus, the spin scattering due to tunneling electrons is on average lower for pump–probe measurements.

Figure 7 shows the behavior of $\tau^*/2$ for different tunneling currents I_t on two ML and three ML of MgO. We find that for spin-polarized tips, the configuration of the tip apex has a negligible influence on $\tau^*/2$ (compare the data for "tip 1" and "tip 2" in Fig. 7). The lines in Fig. 7 show an extrapolation of T_1 reported by Paul *et al.*[13] to the tunneling currents used here.

Despite the differences in the experimental conditions described above, our results for $\tau^*/2$ measured on three ML of MgO are within a factor of ≈3 at the extrapolation of T_1 and show an almost identical current dependency. The difference is larger for the data measured on two ML of MgO, but $\tau^*/2$ again shows a similar trend. Both the trend of the current dependency and the lower times for $\tau^*/2$ are consistent with an increased scattering of tunneling electrons limiting T_1 and suggest that the same is true for $\tau^*/2$.

IV. CONCLUSION

We present a method to achieve a high transmission of RF power to the tip–sample junction of a UHV STM by directly contacting the STM tip through the RF coaxial wiring. As a consequence, a bias modulation at the tip–sample junction is possible at any frequency between DC and 40 GHz. Due to the excellent transmission of the cryogenic part of the wiring, experiments with RF modulation are now possible without significantly heating the ^{3}He stage of our cryostat or reducing its hold time. This constitutes a major improvement over the previous implementation of RF wiring on our machine[3] and other ESR–STM setups,[4] where too high RF losses prevent an RF bias modulation. We demonstrate ESR measurements of Ti on MgO/Ag(100) in frequency sweeps at 0.4 and 4.25 K.

In QSR measurements of the magnetic switching of Fe atoms on MgO/Ag(100), we compare the behavior of the drive frequency at which the system shows the strongest change in its time averaged state occupation with previous measurements of the energy relaxation time T_1.[13] Expressed as a switching time $\tau^*/2$, we find a qualitative similarity in the response of $\tau^*/2$ to the externally applied field, the variation of the STM tunneling current, as well as the thickness of the underlying MgO film. Thus we speculate that $\tau^*/2$ can be used as a measure of intrinsic properties of single atom spin systems, despite the influence of the AC drive signal on its dynamics.

ACKNOWLEDGMENTS

We thank the electronic and mechanical workshops of our institute for their expert assistance. We acknowledge the support from the Swiss National Science Foundation under the following Project Nos.: TMAG-2_209266, 200020_204426, and 200020_176932.

AUTHOR DECLARATIONS

Conflict of Interest

The authors have no conflicts to disclose.

Author Contributions

Johannes Schwenk: Conceptualization (equal); Data curation (equal); Formal analysis (equal); Investigation (equal); Methodology (equal); Project administration (equal); Software (equal); Supervision (equal); Validation (equal); Visualization (equal); Writing – original draft (lead); Writing – review & editing (equal). **Clément M. Soulard**: Conceptualization (equal); Data curation (equal); Formal analysis (equal); Investigation (equal); Methodology (equal); Project administration (equal); Visualization (equal); Writing – original draft (equal). **Shixuan Shan**: Conceptualization (supporting); Data curation (supporting); Formal analysis (supporting); Investigation (supporting); Methodology (supporting); Software (equal); Visualization (equal); Writing – review & editing (supporting). **François Patthey**: Conceptualization (equal); Methodology (supporting); Project administration (supporting); Resources (equal). **Harald Brune**: Conceptualization (lead); Formal analysis (equal); Funding acquisition (lead); Investigation (equal); Project administration (lead); Resources (lead); Supervision (lead); Validation (equal); Writing – original draft (supporting); Writing – review & editing (lead).

DATA AVAILABILITY

The data that support the findings of this study are available from the corresponding authors upon reasonable request.

REFERENCES

[1] W. Paul, S. Baumann, C. P. Lutz, and A. J. Heinrich, "Generation of constant-amplitude radio-frequency sweeps at a tunnel junction for spin resonance STM," Rev. Sci. Instrum. **87**, 074703 (2016).

[2]S. Baumann, W. Paul, T. Choi, C. P. Lutz, A. Ardavan, and A. J. Heinrich, "Electron paramagnetic resonance of individual atoms on a surface," Science **350**, 417–420 (2015).
[3]F. D. Natterer, F. Patthey, T. Bilgeri, P. R. Forrester, N. Weiss, and H. Brune, "Upgrade of a low-temperature scanning tunneling microscope for electron-spin resonance," Rev. Sci. Instrum. **90**, 013706 (2019).
[4]W. M. J. van Weerdenburg, M. Steinbrecher, N. P. E. van Mullekom, J. W. Gerritsen, H. von Allwörden, F. D. Natterer, and A. A. Khajetoorians, "A scanning tunneling microscope capable of electron spin resonance and pump–probe spectroscopy at mK temperature and in vector magnetic field," Rev. Sci. Instrum. **92**, 033906 (2021).
[5]T. S. Seifert, S. Kovarik, C. Nistor, L. Persichetti, S. Stepanow, and P. Gambardella, "Single-atom electron paramagnetic resonance in a scanning tunneling microscope driven by a radio-frequency antenna at 4 K," Phys. Rev. Res. **2**, 013032 (2020).
[6]R. Drost, M. Uhl, P. Kot, J. Siebrecht, A. Schmid, J. Merkt, S. Wünsch, M. Siegel, O. Kieler, R. Kleiner, and C. R. Ast, "Combining electron spin resonance spectroscopy with scanning tunneling microscopy at high magnetic fields," Rev. Sci. Instrum. **93**, 043705 (2022).
[7]J. Hwang, D. Krylov, R. Elbertse, S. Yoon, T. Ahn, J. Oh, L. Fang, W.-j. Jang, F. H. Cho, A. J. Heinrich, and Y. Bae, "Development of a scanning tunneling microscope for variable temperature electron spin resonance," Rev. Sci. Instrum. **93**, 093703 (2022).
[8]Y. Chen, Y. Bae, and A. J. Heinrich, "Harnessing the quantum behavior of spins on surfaces," Adv. Mater. **35**, 2107534 (2023).
[9]L. Claude,"Construction d'un microscope à effet tunnel à basse température et études d'impuretés magnétiques en surfaces," Ph.D. thesis, Swiss Federal Institute of Technology, 2005.
[10]Q. Dubout, "Magnetism of single adatoms and small adsorbed clusters investigated by means of low-temperature STM," Ph.D. thesis, Swiss Federal Institute of Technology, 2013.
[11]M. Hänze, G. McMurtrie, S. Baumann, L. Malavolti, S. N. Coppersmith, and S. Loth, "Quantum stochastic resonance of individual Fe atoms," Sci. Adv. **7**, eabg2616 (2021).
[12]W. M. J. Van Weerdenburg, H. Osterhage, R. Christianen, K. Junghans, E. Domínguez, H. J. Kappen, and A. A. Khajetoorians, "Stochastic syncing in sinusoidally driven atomic orbital memory," ACS Nano **18**, 4840–4846 (2024).
[13]W. Paul, K. Yang, S. Baumann, N. Romming, T. Choi, C. P. Lutz, and A. J. Heinrich, "Control of the millisecond spin lifetime of an electrically probed atom," Nat. Phys. **13**, 403–407 (2017).
[14]F. D. Natterer, F. Donati, F. Patthey, and H. Brune, "Thermal and magnetic-field stability of holmium single-atom magnets," Phys. Rev. Lett. **121**, 027201 (2018).
[15]S. Shan and J. Schwenk, Nanonis-TCP-client, https://github.com/LNS-EPFL/Nanonis-TCP-client.
[16]J. Schwenk and S. Shan, ESR-lib.
[17]Keysight, MXG X-Series N5183B 40 GHz.
[18]Tektronix, AWG5204.
[19]SPECS, Nanonis SPM Control System.
[20]SPECS, Nanonis RC5 SPM controler.
[21]Teledyne Storm Microwave, Duratest 150.
[22]Mini-Circuits, BLK-K44+.
[23]Mini-Circuits, BW-K1-2W44+.
[24]Tektronix, PSPL5361.
[25]Allectra GmbH, 242-SMAD40G-C40-4.
[26]COAX CO., LTD., SC-119/50-SSS-SS.
[27]COAX CO., LTD., SC-119/50-NbTi-NbTi.
[28]EPO-TEK, E4110.
[29]Dynawave, Dynaflex 0.06.
[30]S. Baumann, F. Donati, S. Stepanow, S. Rusponi, W. Paul, S. Gangopadhyay, I. Rau, G. Pacchioni, L. Gragnaniello, M. Pivetta, J. Dreiser, C. Piamonteze, C. Lutz, R. Macfarlane, B. Jones, P. Gambardella, A. Heinrich, and H. Brune, "Origin of perpendicular magnetic anisotropy and large orbital moment in Fe atoms on MgO," Phys. Rev. Lett. **115**, 237202 (2015).
[31]J. Li, W.-D. Schneider, R. Berndt, O. R. Bryant, and S. Crampin, "Surface-state lifetime measured by scanning tunneling spectroscopy," Phys. Rev. Lett. **81**, 4464–4467 (1998).
[32]O. Jeandupeux, L. Bürgi, A. Hirstein, H. Brune, and K. Kern, "Thermal damping of quantum interference patterns of surface-state electrons," Phys. Rev. B **59**, 15926–15934 (1999).
[33]J. Kim, W.-j. Jang, T. H. Bui, D.-J. Choi, C. Wolf, F. Delgado, Y. Chen, D. Krylov, S. Lee, S. Yoon *et al.*, "Spin resonance amplitude and frequency of a single atom on a surface in a vector magnetic field," Phys. Rev. B **104**, 174408 (2021).
[34]B. Wit, R. Vranik, and S. Müllegger, "Enhanced conductance response in radio frequency scanning tunnelling microscopy," Sci. Rep. **12**, 6183 (2022).
[35]U. Fano, "Effects of configuration interaction on intensities and phase shifts," Phys. Rev. **124**, 1866–1878 (1961).
[36]U. Fano, "Sullo spettro di assorbimento dei gas nobili presso il limite dello spettro d'arco," Nuovo Cimento **12**, 154–161 (1935).
[37]Y. Bae, K. Yang, P. Willke, T. Choi, A. J. Heinrich, and C. P. Lutz, "Enhanced quantum coherence in exchange coupled spins via singlet-triplet transitions," Sci. Adv. **4**, eaau4159 (2018).
[38]L. M. Veldman, L. Farinacci, R. Rejali, R. Broekhoven, J. Gobeil, D. Coffey, M. Ternes, and A. F. Otte, "Free coherent evolution of a coupled atomic spin system initialized by electron scattering," Science **372**, 964–968 (2021).
[39]M. Steinbrecher, W. M. J. van Weerdenburg, E. F. Walraven, N. P. E. van Mullekom, J. W. Gerritsen, F. D. Natterer, D. I. Badrtdinov, A. N. Rudenko, V. V. Mazurenko, M. I. Katsnelson, A. van der Avoird, G. C. Groenenboom, and A. A. Khajetoorians, "Quantifying the interplay between fine structure and geometry of an individual molecule on a surface," Phys. Rev. B **103**, 155405 (2021).
[40]K. Yang, Y. Bae, W. Paul, F. D. Natterer, P. Willke, J. L. Lado, A. Ferrón, T. Choi, J. Fernández-Rossier, A. J. Heinrich, and C. P. Lutz, "Engineering the eigenstates of coupled spin-1/2 atoms on a surface," Phys. Rev. Lett. **119**, 227206 (2017).
[41]K. Yang, W. Paul, F. D. Natterer, J. L. Lado, Y. Bae, P. Willke, T. Choi, A. Ferrón, J. Fernández-Rossier, A. J. Heinrich, and C. P. Lutz, "Tuning the exchange bias on a single atom from 1 mT to 10 T," Phys. Rev. Lett. **122**, 227203 (2019).
[42]R. Kawaguchi, K. Hashimoto, T. Kakudate, K. Katoh, M. Yamashita, and T. Komeda, "Spatially resolving electron spin resonance of π-radical in single-molecule magnet," Nano Lett. **23**, 213–219 (2022).
[43]T. S. Seifert, S. Kovarik, D. M. Juraschek, N. A. Spaldin, P. Gambardella, and S. Stepanow, "Longitudinal and transverse electron paramagnetic resonance in a scanning tunneling microscope," Sci. Adv. **6**, eabc5511 (2020).